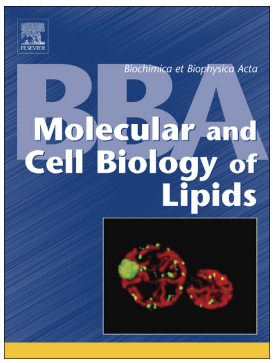

The N-terminal homology (ENTH) domain of Epsin 1 is a sensitive reporter of physiological PI(4,5)P2 dynamics

Michael G. Leitner, Veronika Thallmair, Bettina U. Wilke, Valentin Neubert, Yannick Kronimus, Christian R. Halaszovich, Dominik Oliver

PII: S1388-1981(18)30204-X
DOI: doi:10.1016/j.bbalip.2018.08.005
Reference: BBAMCB 58346

To appear in: *BBA - Molecular and Cell Biology of Lipids*

Received date: 2 March 2018
Revised date: 18 June 2018
Accepted date: 4 August 2018

Please cite this article as: Michael G. Leitner, Veronika Thallmair, Bettina U. Wilke, Valentin Neubert, Yannick Kronimus, Christian R. Halaszovich, Dominik Oliver , The N-terminal homology (ENTH) domain of Epsin 1 is a sensitive reporter of physiological PI(4,5)P2 dynamics. Bbamcb (2018), doi:10.1016/j.bbalip.2018.08.005

Title Page

The N-terminal homology (ENTH) domain of Epsin 1 is a sensitive reporter of physiological PI(4,5)P_2 dynamics

Michael G. Leitner[1,2,*], Veronika Thallmair[2], Bettina U. Wilke[2], Valentin Neubert[2], Yannick Kronimus[2], Christian R. Halaszovich[2], and Dominik Oliver[2,3,4]

[1]Division of Physiology, Department of Physiology and Medical Physics, Innsbruck Medical University, 6020 Innsbruck, Austria

[1]Department of Neurophysiology, Institute of Physiology and Pathophysiology, Philipps-University Marburg, 35037 Marburg, Germany

[3]DFG Research Training Group, Membrane Plasticity in Tissue Development and Remodeling, GRK 2213, Philipps University, Germany.

[4]Center for Mind, Brain and Behavior (CMBB), Universities of Marburg and Giessen, Germany

Mailing addresses of all authors:

Michael.Leitner@i-med.ac.at (M.G.L), veronika.thallmair@uni-marburg.de (V.T), Wilkebet@staff.uni-marburg.de (B.U.W), valentin.neubert@staff.uni-marburg.de (V.N), Yannick.Kronimus@uk-essen.de (Y.K), Halaszov@staff.uni-marburg.de (C.R.H), oliverd@staff.uni-marburg.de (O.D)

***Address correspondence to:**

Dr. Michael G. Leitner

Division of Physiology

Department of Physiology and Medical Physics

Schöpfstraße 41/EG

6020 Innsbruck

Austria

E-Mail: Michael.Leitner@i-med.ac.at

Tel.: +43 (0) 512 9003 70843

Running title: ENTH-GFP detects physiological PI(4,5)P_2 dynamics with high sensitivity

Abbreviations: Ci-VSP, *Ciona intestinalis* voltage-sensing phosphatase; ENTH, epsin N-terminal homology; GFP, green fluorescent protein; G_qPCR, G_q protein-coupled receptor; m1R, muscarinic receptor type 1; Oxo-M, oxotremorine-M; PH, pleckstrin homology; PI, phosphoinositide; PI(4,5)P_2, phosphatidylinositol-(4,5)-bisphosphate; PI(4)P, phosphatidylinositol-(4)-phosphate; PLC, phospholipase C; RFP, red fluorescent protein; TIRF, total internal reflection fluorescence;

ABSTRACT

Phospholipase Cβ (PLCβ)-induced depletion of phosphatidylinositol-(4,5)-bisphosphate ($PI(4,5)P_2$) transduces a plethora of signals into cellular responses. Importance and diversity of $PI(4,5)P_2$-dependent processes led to strong need for biosensors of physiological $PI(4,5)P_2$ dynamics applicable in live-cell experiments. Membrane $PI(4,5)P_2$ can be monitored with fluorescently-labeled phosphoinositide (PI) binding domains that associate to the membrane depending on $PI(4,5)P_2$ levels. The pleckstrin homology domain of PLCδ1 (PLCδ1-PH) and the C-terminus of tubby protein ($tubby_{CT}$) are two such sensors widely used to study $PI(4,5)P_2$ signaling. However, certain limitations apply to both: PLCδ1-PH binds cytoplasmic inositol-1,4,5-trisphosphate (IP_3) produced from $PI(4,5)P_2$ through PLCβ, and $tubby_{CT}$ responses do not faithfully report on PLCβ-dependent $PI(4,5)P_2$ dynamics. In searching for an improved biosensor, we fused N-terminal homology domain of epsin1 (ENTH) to GFP and examined use of this construct as genetically-encoded biosensor for $PI(4,5)P_2$ dynamics in living cells. We utilized recombinant tools to manipulate PI or G_q protein-coupled receptors (G_qPCR) to stimulate PLCβ signaling and characterized PI binding properties of ENTH-GFP with total internal reflection (TIRF) and confocal microscopy. ENTH-GFP specifically recognized membrane $PI(4,5)P_2$ without interacting with IP_3, as demonstrated by dialysis of cells with the messenger through a patch pipette. Utilizing Ci-VSP to titrate $PI(4,5)P_2$ levels, we found that ENTH-GFP had low $PI(4,5)P_2$ affinity. Accordingly, ENTH-GFP was highly sensitive to PLCβ-dependent $PI(4,5)P_2$ depletion, and in contrast to PLCδ1-PH, overexpression of ENTH-GFP did not attenuate G_qPCR signaling. Taken together, ENTH-GFP detects minute changes of $PI(4,5)P_2$ levels and provides an important complementation of experimentally useful reporters of $PI(4,5)P_2$ dynamics in physiological pathways.

Keywords: epsin N-terminal homology, G_q protein-coupled receptor, phosphatidylinositol-(4,5)-bisphosphate, phospholipase C, tubby protein, PLCδ1-PH, pleckstrin homology, signal transduction, phospholipids, Ci-VSP

1. INTRODUCTION

Stimulation of G_q protein-coupled receptors (G_qPCR) activates phospholipase Cβ (PLCβ), thereby inducing enzymatic hydrolysis of phosphatidylinositol-(4,5)-bisphosphate ($PI(4,5)P_2$) into diacylglycerol (DAG) and inositol-1,4,5-trisphosphate (IP_3). Membrane-associated $PI(4,5)P_2$ not only serves as precursor of the cellular messengers DAG and IP_3, but also directly controls activity of many ion channels and transporters, modulates protein trafficking and coordinates membrane association of the cytoskeleton [1-5]. Accordingly, depletion of $PI(4,5)P_2$ through receptor-triggered activation of PLCβ couples a plethora of extracellular stimuli to cellular physiology.

$PI(4,5)P_2$ dynamics can be monitored with phosphoinositide (PI) recognition domains fused to fluorescent proteins [1, 6, 7]. These reporters associate to the plasma membrane, when $PI(4,5)P_2$ levels are high, and translocate into the cytoplasm upon $PI(4,5)P_2$ depletion. Consequently, changes of fluorescence intensities at the plasma membrane or in the cytoplasm report on $PI(4,5)P_2$ concentration dynamics [6, 7]. Established sensors of membrane $PI(4,5)P_2$ are based on the pleckstrin homology (PH) domain of PLCδ1 (PLCδ1-PH) [8, 9] and the C-terminal domain of $PI(4,5)P_2$-binding protein tubby ($tubby_{CT}$) [10-13]. Although many studies have employed PLCδ1-PH or (less frequently) $tubby_{CT}$ to monitor cellular $PI(4,5)P_2$, certain drawbacks of both sensors need consideration. PLCδ1-PH not only binds $PI(4,5)P_2$ but also IP_3, and thus dissociates from the plasma membrane because of competitive binding to cytoplasmic IP_3. Depending on the actual $PI(4,5)P_2/IP_3$ ratio resulting from PLC activation, this may lead to overestimation of PLCβ-mediated $PI(4,5)P_2$ depletion [12, 14-17]. Accordingly, PLCδ1-PH can rather be considered as a biosensor of PLCβ activity during stimulation of G_qPCR than a reporter for actual $PI(4,5)P_2$ depletion. Furthermore, as due to its high $PI(4,5)P_2$ affinity PLCδ1-PH competes for $PI(4,5)P_2$ binding with endogenous proteins, overexpression of this construct interferes with $PI(4,5)P_2$-dependent processes. E.g., overexpression of PLCδ1-PH abrogated $PI(4,5)P_2$-mediated contacts between plasma membrane and cytoskeleton, thereby altering the morphology of transfected cells [3]. Similarly, overexpression of both PLCδ1-PH and $tubby_{CT}$ attenuated PLCβ-mediated Ca^{2+}-transients during stimulation of G_qPCRs, likely by shielding $PI(4,5)P_2$ from PLCβ, and in case of PLCδ1-PH also through chelation of IP_3 [12, 13]. On the other hand, membrane association of $tubby_{CT}$ was largely insensitive to conditions expected to result in substantial depletion of $PI(4,5)P_2$, i.e. $tubby_{CT}$ did not dissociate from the plasma membrane despite massive activation of PLCβ under various experimental conditions [11-13]. Based on this very low sensitivity, it has been proposed that the $PI(4,5)P_2$ binding affinity of $tubby_{CT}$ is relatively

high such that residual $PI(4,5)P_2$ suffices to keep $tubby_{CT}$ at the plasma membrane during stimulation of G_qPCR and PLCβ [11-13]. However, gradual titration of membrane $PI(4,5)P_2$ with the voltage-sensitive PI phosphatase of *Ciona intestinalis* (Ci-VSP) rather indicated that $tubby_{CT}$ actually has a lower $PI(4,5)P_2$ binding affinity than PLCδ1-PH [18]. Therefore, additional yet unknown interactions apart from $PI(4,5)P_2$ binding may determine the responses of $tubby_{CT}$ to stimulation of G_qPCR/PLCβ.

Recently, the epsin1 N-terminal homology (epsin1-ENTH) domain was introduced as alternative sensor for cellular $PI(4,5)P_2$ [19]. Yoon and colleagues covalently labelled epsin1-ENTH with a fluorophore sensitive to the lipid environment (termed DAN-eENTH) allowing for quantitative analysis of $PI(4,5)P_2$ dynamics by monitoring changes of the fluorophore´s spectral properties [19]. However, applicability of this approach may be limited, as besides chemical modification, introduction of DAN-eENTH into living cells, e.g. by microinjection, is technically demanding, may be restricted to certain cell types and may even affect cell viability. We reasoned that despite elegant design and quantitative nature of the DAN-eENTH approach, usage of GFP-fused epsin1-ENTH as a genetically-encoded $PI(4,5)P_2$ translocation sensor may be more straightforward in many experimental settings. Moreover, since epsin1-ENTH is structurally not related to PLCδ1-PH and $tubby_{CT}$ [10, 19, 20], its use as a live-cell sensor may not be compromised by the abovementioned problems associated with these $PI(4,5)P_2$ binding domains. We thus fused green fluorescent protein (GFP) to epsin1-ENTH and characterized PI binding characteristics of this reporter (ENTH-GFP) in living cells. ENTH-GFP specifically recognized $PI(4,5)P_2$ and did not interact with other membrane PI nor cytoplasmic IP_3. ENTH-GFP exhibited low apparent affinity for $PI(4,5)P_2$ and reported on G_qPCR-triggered activation of PLCβ even at very low agonist concentrations. Consistent with its low $PI(4,5)P_2$ affinity, overexpression of the sensor did not affect $PI(4,5)P_2$ dynamics or G_qPCR signaling. We conclude that ENTH-GFP is a highly sensitive biosensor and a valuable complement of the available set of reporters for monitoring physiological $PI(4,5)P_2$ dynamics in cellular pathways.

2. MATERIAL AND METHODS

2.1 Cell Culture, Transfection and Mutagenesis

Chinese hamster ovary/dhFr- cells (CHO) were kept in MEM Alpha Medium supplemented with 10% fetal calf serum (FCS) and 1% penicillin/streptomycin (all Invitrogen GmbH, Darmstadt, Germany). In preparation of experiments presented in Figure 3A, cells were kept in serum free media for 24 h prior to experiments (serum-starved). Cells were transfected with jetPEI (Polyplus Transfection, Illkirch, France) and all experiments were performed 24 h-48 h

after transfection at room temperature (22-25°C). Cells were perfused throughout experiments with extracellular solution containing (mM) 144 NaCl, 5.8 KCl, 1.3 $CaCl_2$, 0.9 $MgCl_2$, 0.7 NaH_2PO_4, 10 HEPES and 5.6 D-glucose, pH 7.4 (with NaOH), 305-310 mOsm/kg. The expression vectors used were: epsin1-ENTH-pEGFP-N1 (amino acids 1-158; UniProt accession: O88339;[19]), PLCδ1-PH-pEGFP-N1 (1-170; P51178), $tubby_{CT}$-pEGFP-C1 (243-505; P50586), Btk-PH-pEGFP-N1 (1-177; Q06187), P4M-SidM-pEGFP-C1 (1x; Q5ZSQ3 [21]), Ci-VSP-pRFP-C1 (Q4W8A1), human muscarinic receptor 1 (hm1R)-pSGHV0 (Q96RH1), KCNQ2-pBK-CMV (K_v7.2, O43526), KCNQ3-pBK-CMV (K_v7.3, O43525), Lyn11-FRB-pRFP-N1 (1-10; P07948), CFP-FKBP-Inp54p (1-331; Q08227), CFP-FKBP-PIPK (O70161), pEGFP-C1 (transfection control; Addgene, Teddington, UK). In experiments presented in Figure 5, cells were transfected with equal amounts of plasmid DNA encoding KCNQ2 channels (co-expression of free EGFP served as control). Point mutations ($tubby_{CT}$(R332H)-GFP and ENTH(S4W)-GFP) were introduced with the QuickChangeII XL Site-Directed mutagenesis kit (Stratagene, Santa Clara, CA).

2.2 Confocal Microscopy

Confocal imaging was performed with an upright LSM 710 - Axio Examiner.Z1 microscope equipped with a W Plan/Apochromat 20x/1.0 DIC M27 75 mm water immersion objective (Zeiss, Jena, Germany) [22]. Red fluorescent protein (RFP) was excited at 561 nm with a DPSS 561-10 laser (Zeiss) and fluorescence emission was sampled at 582-754 nm. The sample interval for time series was 4 s. Green fluorescent protein (GFP) was excited at 488 nm with an argon laser and fluorescence emission was recorded at 493-597 nm.

2.3 Total Internal Reflection Fluorescence (TIRF) Microscopy

The majority of TIRF experiments was carried-out on an upright BX51WI microscope with a TIRF-condenser (numerical aperture of 1.45; both Olympus, Hamburg, Germany) and a 488 nm laser (20 mW; Picarro, Sunnyvale, CA) [23]. Fluorescence was imaged with a LUMPlanFI/IR 40X/0.8 water immersion objective (Olympus), and sampled with an IMAGO-QE cooled CCD camera controlled by TILLvisION software (TILL Photonics, Gräfelfing, Germany). CHO cells co-expressing Ci-VSP (Figure 3D-G) and cells dialyzed with IP_3 (Figure 2; Sigma-Aldrich, Munich, Germany) were imaged and voltage-clamped simultaneously. Cells expressing Ci-VSP were chosen based on membrane RFP fluorescence associated with expression of Ci-VSP-pRFP-C1. Sample interval for imaging time series was 4 s. F/F_0 traces were calculated pixel-wise from the background-corrected TIRF signal (F) and basal fluorescence intensity (F_0), averaged over the footprint of a cell excluding cell margins to prevent movement artifacts.

For experiments shown in Figure 3D, a custom-built inverted TIRF setup was used: a Nikon Eclipse Ti inverted microscope was equipped with an Apo TIRF 100x/1.49 oil immersion objective, a 488 nm laser (200 mW, iBeam smart; Toptica Photonics AG, Gräfelfing, Germany) and a TIRF condenser (Rapp OptoElectronic, Wedel, Germany). TIRF images were acquired with a CoolSnap HQ2 camera (Photometrics, Tuscon, AZ, USA) that also controlled the laser shutter (nmLaser Products Inc., San José, CA, USA). Image acquisition was performed with µ-Manager software [24].

2.4 Electrophysiological Experiments

Whole cell KCNQ (K_v7) currents were recorded with an Axopatch 200B amplifier (Molecular Devices, Union City, CA) in voltage-clamp mode [25]. Data were sampled with an ITC-18 interface and controlled by PatchMaster software (both HEKA Elektronik, Lambrecht, Germany). Currents were low-pass filtered at 2 kHz, sampled at 5 kHz and normalized to the cell capacitance (current density; pA/pF). Patch pipettes were pulled from borosilicate glass (Sutter Instrument Company, Novato, CA, USA) and had an open pipette resistance of 2-3 MΩ after back-filling with intracellular solution containing (mM) 135 KCl, 2.41 $CaCl_2$, 3.5 $MgCl_2$, 5 HEPES, 5 EGTA, 2.5 Na_2ATP, 0.1 Na_3GTP, pH 7.3 (with KOH), 290-295 mOsm/kg. Series resistance (R_s) typically was below 6 MΩ and compensated for throughout the recordings (80-90%). Liquid junction potentials (approx. -4 mV) were not compensated. For IP_3 dialysis and fluorescence voltage curves, cells were whole cell voltage-clamped with an EPC-10 amplifier controlled by PatchMaster software (both HEKA). IP_3 was added at 5 µM to the internal solution, and cells were kept in the whole cell configuration at -60 mV for at least 5 minutes. To ensure rapid dialysis of the cells with IP_3, R_s was kept below 5 MΩ in these experiments.

For steady-state fluorescence-voltage (F-V) relations, Ci-VSP was activated by voltage steps from -60 mV (-80 mV for ENTH(S4W)-GFP) to +80 mV (+20 mV increments for 60 s each). Data obtained from single cells were fitted with a Boltzmann function $F=F_{min}+(F_{max}-F_{min})/[1 + \exp((V-V_h)/s))]$, where F was the recorded TIRF intensity, V was the holding potential, V_h was the voltage at the half-maximal response, and s described the steepness of the curve [18, 23]. Data were normalized as follows: F_{min} was subtracted from the data and the result was normalized to F_{max}-F_{min}: $F_{norm}=(F-F_{min})/(F_{max}-F_{min})$. F_{min} and F_{max} were derived from the fit for each individual cell before averaging. Thus, F_{norm} approaches unity as V approaches negative infinity (phosphatase activity approaches zero), and F_{norm} approaches zero for large positive voltages (phosphatase activity approaches maximum).

2.5 Reagents and dose-response relations

Human insulin-like growth factor 1 (Sigma), rapamycin (solution in Me_2SO, Merck KGaA, Darmstadt, Germany), oxotremorine-M (Oxo-M; Biotrend Chemikalien GmbH, Köln, Germany), and GSK-A1 (SYNkinase, Parkville, Australia) were applied via a custom-built gravity-based application system. Dose-response relations were derived from I/I_0 KCNQ (K_v7) currents at 0 mV and from F/F_0 TIRF signals at increasing Oxo-M concentrations. Responses were fitted with a Hill equation with $F/F_b = F_b+(F_{max}-F_b)/(1+(EC_{50}/[S])^n)$, where F is the normalized current/TIRF signal, F_b and F_{max} denote the minimal and maximal current/TIRF signal at low and high agonist concentration, EC_{50} is the concentration at the half maximal effect, [S] is the oxo-M concentration and n is the Hill coefficient [26]. Curves were normalized to I_{max}-I_{min} for current recordings and F_{max}-F_{min} for TIRF recordings as derived from fits of individual cells.

2.6 Statistical Analysis

Data were analyzed using TILLvisION (TILL Photonics), Zen2009 (Zeiss, Jena, Germany), ImageJ (National Institute of Health, Bethesda, USA), Igor Pro (Wavemetrics, Lake Oswego, OR) and PatchMaster (HEKA). Statistical analysis was performed with two-tailed Student´s, Wilcoxon signed, Dunnett or Scheffé test. Statistical significance was assigned at $P \leq 0.05$ (* $P \leq 0.05$, ** $P \leq 0.01$, *** $P \leq 0.001$). All data are presented as mean ± SEM. In electrophysiological experiments, *n* represents the number of individual cells recorded from at least three independent experiments (independent transfections, i.e. biological replicates). In imaging experiments, *n* represents the number of individual cells obtained from at least four independent experiments. Data presented in Figure 3D were obtained in three independent experiments

3. RESULTS

We evaluated applicability of Epsin1-ENTH-GFP (termed ENTH-GFP) as a genetically-encoded reporter for G_qPCR-triggered $PI(4,5)P_2$ dynamics in comparison to PLCδ1-PH-GFP, $tubby_{CT}$-GFP, and two mutants, $tubby_{CT}$(R332H)-GFP and ENTH(S4W)-GFP, that presumably exhibit lower $PI(4,5)P_2$ binding affinities compared to the wild type domains [11, 19].

3.1 ENTH-GFP exhibits low degree of membrane association

Using confocal microscopy, we first characterized subcellular localization of ENTH-GFP in transiently transfected CHO cells. In these experiments, we co-expressed Lyn11-RFP [27] to visualize the plasma membrane together with GFP-labelled PI binding domains. Membrane association of both ENTH-GFP and ENTH(S4W)-GFP was low, and we always detected a

large fraction of the associated GFP fluorescence in the cytoplasm of resting cells (Figure 1A, B). Cells expressing ENTH-GFP appeared healthy and the sensor was not bound to intracellular membranes in most cells (Figure 1A, B). However, in approximately one third of all cells ENTH-GFP labelled rod-like structures in the cytoplasm (Figure 1B). Figure 1A shows that in comparison to established $PI(4,5)P_2$ sensors membrane association of ENTH-GFP and ENTH(S4W)-GFP was lower than that of PLCδ1-PH-GFP and $tubby_{CT}$-GFP, but more similar to mutant $tubby_{CT}$(R332H)-GFP.

3.2 ENTH-GFP and ENTH(S4W)-GFP reliably detect receptor-triggered activation of PLCβ

We then set out to analyse whether ENTH-GFP qualifies as translocation sensor of PLCβ-dependent $PI(4,5)P_2$ depletion. To this end, we overexpressed G_q-coupled muscarinic receptor type 1 (m1R) in CHO cells and activated these receptors by extracellular application of a saturating concentration of oxotremorine-M (Oxo-M; 10 µM) [28]. Overexpression of m1R reconstitutes G_qPCR signalling in cultured cells, serving as an accepted model for this signalling pathway [28-32]. Membrane association of PI-binding domains was measured with total internal reflection fluorescence (TIRF) or confocal microscopy [23, 33].

As observed with TIRF microscopy, membrane association of ENTH-GFP and ENTH(S4W)-GFP readily decreased upon activation of m1R through Oxo-M (10 µM), and both sensors returned to the membrane within few minutes after wash-out of the agonist (Figure 1C). Relative changes in membrane association of ENTH-GFP(S4W) were smaller than that of the wild type sensor domain ($P \leq 0.001$; Figure 1E). During activation of m1R, we detected a corresponding cytoplasmic increase of ENTH-GFP- and ENTH(S4W)-GFP-associated fluorescence, when using confocal microscopy to measure location of the sensors in the cytoplasm (Figure 1F). Both observations are consistent with $PI(4,5)P_2$-dependent reversible membrane association during G_qPCR activation and in particular with dissociation from the membrane as result of PLCβ-mediated $PI(4,5)P_2$ depletion. To verify $PI(4,5)P_2$ depletion under the specific experimental conditions, we utilized $PI(4,5)P_2$-dependent KCNQ (K_v7) potassium (K^+) ion channels, as G_qPCR-mediated inhibition of these channels mainly depends on PLCβ-dependent $PI(4,5)P_2$ depletion [30, 34-36]. We observed strong reduction of KCNQ-mediated currents, when activating m1R (Supplemental Figure 1A) confirming the expected $PI(4,5)P_2$ depletion. As shown previously, PLCδ1-PH-GFP [8, 9], but not $tubby_{CT}$ [11-13], strongly and reversibly dissociated from the membrane during application of Oxo-M in cells co-expressing m1R (Figure 1D). Paradoxically, $tubby_{CT}$ even exhibited a transient increase of membrane association during activation of the G_qPCR (Figure 1D). However, in line with

previous reports [11-13], the tubby$_{CT}$(R332H)-GFP mutant translocated from the plasma membrane during activation of m1R, likely due to reduced PI(4,5)P_2 affinity, thus reporting on PLCβ-induced PI(4,5)P_2 depletion.

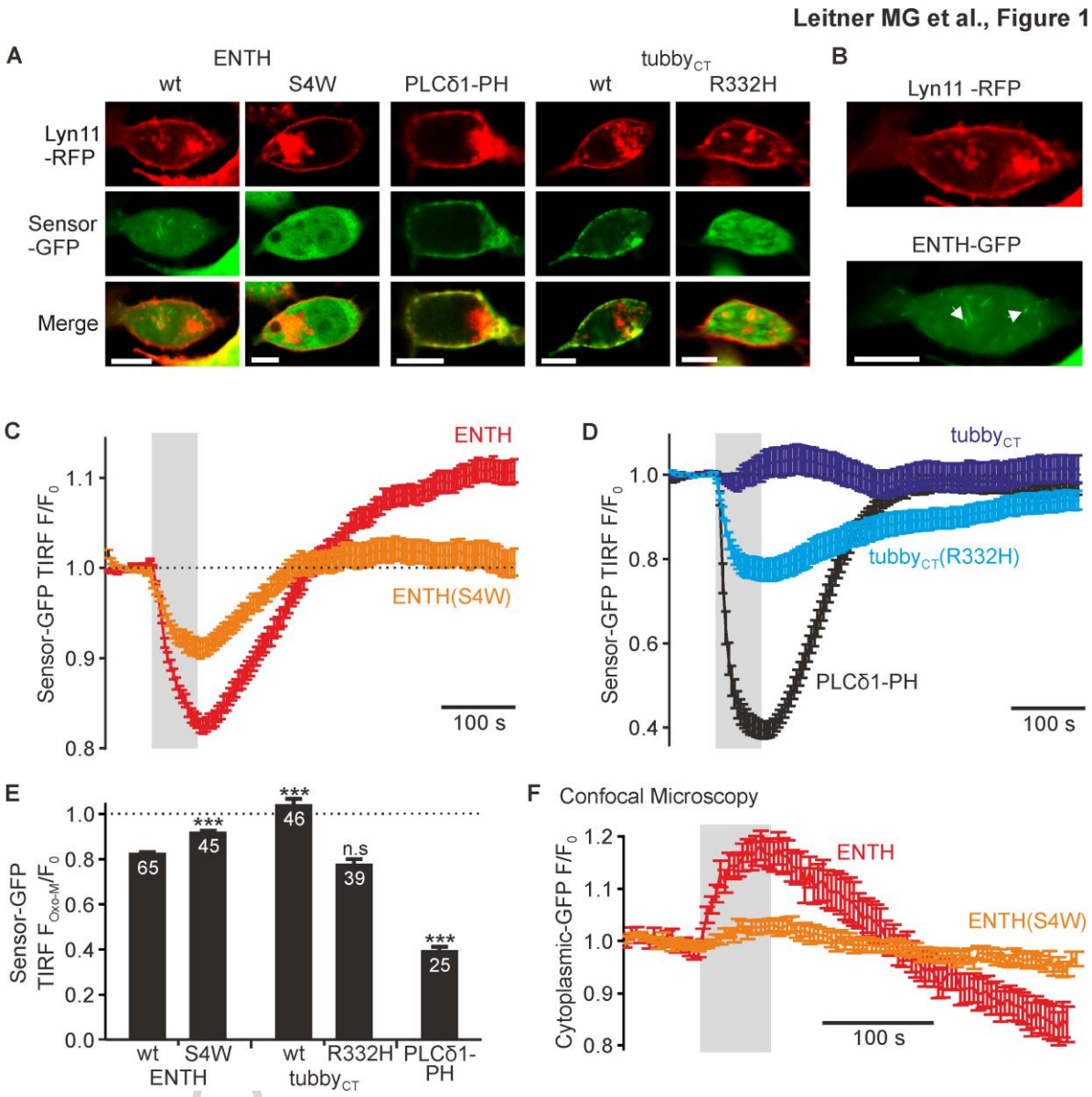

Figure 1. ENTH-GFP is a reliable biosensor of PLCβ activity in living cells.
(A) Confocal images of CHO cells transiently expressing Lyn11-RFP (*red*) together with PI recognition domains fused to GFP (*green*). We detected large amounts of ENTH-GFP, ENTH(S4W) and tubby$_{CT}$(R332H)-GFP in the cytoplasm of resting cells (all scale bars 10 µm). **(B)** In some cells, ENTH-GFP labelled rod-like intracellular structures (*see arrowheads*; images are the same as shown in (A); scale bar 10 µm). **(C)** Stimulation of m1R with Oxo-M (10 µM) induced robust and reversible membrane dissociation of ENTH-GFP (n=65) and ENTH(S4W)-GFP (n=45). **(D)** Membrane-association of PLCδ1-PH-GFP (n=25) and tubby$_{CT}$(R332H)-GFP (n=39) reversibly decreased in response to m1R activation. Tubby$_{CT}$-GFP (n=46) displayed a transient increase of membrane association during activation of m1R. Traces in (C+D) show mean time course of membrane binding recorded with TIRF microscopy. **(E)** Measured with TIRF microscopy, relative changes of membrane association of ENTH-GFP were bigger than for ENTH(S4W) (P≤0.001) and for tubby$_{CT}$ (P≤0.001), similar to tubby$_{CT}$(R332H)-GFP (n.s, not significant) and smaller than for PLCδ1-PH-GFP

(P≤0.001; changes of membrane association derived from experiments shown in (C) and (D)). **(F)** We detected a cytoplasmic increase of ENTH-GFP (n=14) and ENTH(S4W)-GFP (n=26) during activation of m1R using confocal microscopy to measure sensor location in the cytoplasm. Grey insets in (C), (D) and (F) indicate application of Oxo-M (10 µM).

In these experiments, relative changes in membrane association of ENTH-GFP were similar to tubby$_{CT}$(R332H)-GFP (not significant; P>0.05), but smaller than of PLCδ1-PH-GFP (P≤0.001; Figure 1E). Taken together, these experiments demonstrated that ENTH-GFP responses reflect membrane PI(4,5)P_2 dynamics in a robust, although relatively small translocation signal. We attribute the small signal to the low degree of membrane association at rest, which must set the upper limit on the amount of fluorescent sensors that can translocate to the cytosol.

3.3 ENTH-GFP localization is unaffected by cytoplasmic IP$_3$

We next analyzed whether ENTH-GFP translocation indeed selectively depends on PI(4,5)P_2 depletion during activation of G_qPCRs. To test for potential influence of cytoplasmic IP_3 on membrane association of ENTH-GFP, we dialyzed cells with IP_3 through a patch pipette (Figure 2A). Even in absence of IP_3, membrane association of all sensors tested, including ENTH (wild type and mutant), PLCδ1-PH-GFP and tubby$_{CT}$, decreased upon establishment of the whole cell configuration, presumably due to diffusion of sensors into the patch pipette following rupture of the membrane patch (Figure 2B-D) [c.f. 22]. Membrane association of PLCδ1-PH-GFP decreased even further (P ≤ 0.001; Figure 2B and D), when 5 µM IP_3 was supplied via the pipette solution. This result is explained by binding of PLCδ1-PH-GFP to IP_3 [see also e.g. 15], competition of IP_3 with binding to PI(4,5)P_2 and hence dissociation of the sensor from the membrane. In contrast, membrane localization of ENTH-GFP and tubby$_{CT}$-GFP was not affected by dialysis of cells with 5 µM IP_3 (Figure 2B, C) [for tubbyCT c.f. 11]. This indicated that ENTH-GFP does not bind IP_3 in the living cell, consistent with lack of IP_3 binding *in vitro* [19].

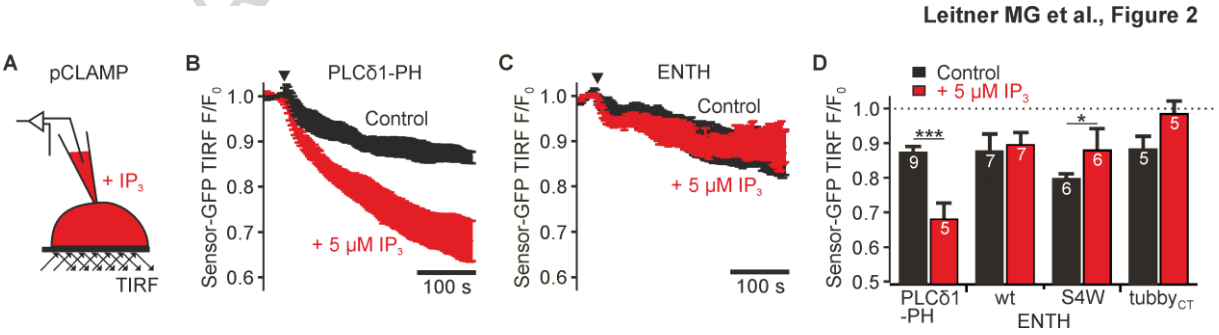

Figure 2. Membrane association of ENTH-GFP is not affected by cytoplasmic IP$_3$. **(A)** Membrane association of PI recognition domains was recorded with TIRF microscopy in cells dialyzed with intracellular solution containing 5 µM IP_3 through a patch pipette (see

"Material and Methods" for details). **(B-D)** Even in absence of IP_3, membrane association of all sensors decreased upon establishment of the whole cell configuration (*black*, cells dialyzed with standard intracellular solution). The *arrowhead* in (B) and (C) indicates establishment of the whole cell configuration. **(B)** Membrane association of PLCδ1-PH-GFP decreased even further, when cells were dialyzed with pipette solution containing IP_3 (*red*). **(C)** membrane localization of ENTH-GFP was insensitive to cytoplasmic IP_3. **(D)** shows a summary of recordings as shown in (B) and (C). Membrane association of ENTH-GFP and $tubby_{CT}$ constructs was not affected by dialysis of cells with IP_3. Upon dialysis of cells with IP_3, membrane association of PLCδ1-PH-GFP significantly decreased ($P \leq 0.001$) and of ENTH(S4W)-GFP surprisingly increased ($P \leq 0.05$) (TIRF signals were analyzed after 5 min of dialysis of cells with control solution or with solution containing 5 µM IP_3 (*red*); numbers in (D) represent numbers of cells recorded for each experimental condition).

3.4 ENTH-GFP exhibits high PI(4,5)P_2 binding specificity and low affinity in living cells

In vitro, Epsin1-ENTH binds to PI(4,5)P_2, but also to PI(3,4,5)P_3 and PI(3,4)P_2 [19, 20]. Because specificity of PI binding domains *in vitro* can differ substantially from their behavior in the living cell [37, 38], we next aimed at characterizing PI binding of ENTH-GFP in cells.

First, we investigated potential binding of ENTH-GFP to 3-phosphorylated PI(3,4,5)P_3 and PI(3,4)P_2. Because cellular resting concentrations of these PIs are low [1], we increased levels of PI(3,4,5)P_3 and PI(3,4)P_2 experimentally to address interaction with ENTH-GFP. To this end, we treated serum-starved CHO cells with insulin-like growth factor (IGF-1; 0.4 µg/ml) to activate PI3-kinases through endogenous IGF receptors [18, 39]. Stimulation of IGF receptors increased cellular PI(3,4,5)P_3 levels within a couple of minutes as monitored by membrane recruitment of PI(3,4,5)P_3-specific probe Btk-PH-GFP during IFG-1 application (TIRF $F_{IGF\text{-}1}/F_0$ 1.32 ±0.03; n=31; Figure 3A) [18, 40]. In analogous experiments, membrane association of ENTH-GFP increased by only about 3% during IGF-1 treatment (Figure 3A; TIRF $F_{IGF\text{-}1}/F_0$ 1.03 ±0.01, n=64). These findings demonstrated that in contrast to *in vitro* binding assays, ENTH-GFP binds only weakly to PI(3,4,5)P_3 in living cells. As treatment with IGF-1 has been shown to also increase PI(3,4)P_2 levels in CHO cells [39], these experiments also indicated that ENTH-GFP does not relevantly bind to PI(3,4)P_2 in living cells.

We additionally utilized genetically-encoded tools for experimental manipulation of other PI species. A rapamycin-induced dimerization strategy was employed to recruit enzymes to the plasma membrane that metabolize PI(4,5)P_2 and PI(4)P [41, 42]. As shown in Figure 3B, rapamycin-induced membrane recruitment of 5-phosphatase Inp54p that specifically dephosphorylates PI(4,5)P_2 to PI(4)P caused strong membrane dissociation of ENTH-GFP (TIRF F_{Inp54p}/F_0 0.79 ±0.02; n=35). Noteworthy, the extent of Inp54p-induced translocation of

ENTH-GFP was similar to its membrane dissociation during stimulation of m1R (c.f. Figure 1C) and qualitatively similar to PLCδ1-PH-GFP responses previously published with the same Inp54p/rapamycin system [41-43]. When we recruited PI(4)P-5-kinase (PI(4)P-5K) to the membrane that synthesizes $PI(4,5)P_2$ from PI(4)P [41], membrane association of ENTH-GFP increased (Figure 3C; ENTH-GFP TIRF $F_{PI(4)P\text{-}5K}/F_0$: 1.09 ±0.01, n=42) demonstrating that ENTH-GFP also recognizes an increase of $PI(4,5)P_2$ in the plasma membrane. This PI(4)P-5K-induced increase of membrane association of ENTH-GFP was significantly higher than that of PLCδ1-PH-GFP in analogous experiments (Figure 3C; PLCδ1-PH-GFP TIRF $F_{PI(4)P\text{-}5K}/F_0$: 1.06 ±0.01, n=27; $P \leq 0.05$; TIRF F/F_0 values after 100 s of rapamycin application were compared). As both enzymes (Inp54p and PI(4)P-5K) interconvert $PI(4,5)P_2$ and PI(4)P stoichiometrically [41, 42], these findings demonstrate that ENTH-GFP strongly prefers $PI(4,5)P_2$ over PI(4)P. To further scrutinize potential binding of ENTH-GFP to PI(4)P, we used GSK-A1 [44-47], a specific inhibitor of type-III PI 4-kinases (PI4IIIK) that mediate synthesis of PI(4)P [1]. Application of GSK-A1 (10 nM) induced rapid membrane dissociation of PI(4)P-specific reporter P4M-SidM-GFP [21] (TIRF $F_{GSK\text{-}A1}/F_0$: 0.84 ±0.02, n=14; $P \leq 0.001$ compared to baseline; Figure 3D). In contrast, membrane association of PLCδ1-PH-GFP was not significantly changed through treatment with GSK-A1 (TIRF $F_{GSK\text{-}A1}/F_0$: 0.96 ±0.02, n=11; not significant change compared to baseline; Figure 3D). Thus consistent with previous reports [45, 47], GSK-A1 caused depletion of PI(4)P without changing $PI(4,5)P_2$ levels in CHO cells (Figure 3D). Membrane association of ENTH-GFP was also not affected by inhibition of PI4IIIK through GSK-A1 (10 nM) (TIRF $F_{GSK\text{-}A1}/F_0$: 0.99 ±0.01, n=11; not significant change compared to baseline; Figure 3D), unequivocally demonstrating that ENTH-GFP does not bind to PI(4)P in the plasma membrane.

To quantitatively define $PI(4,5)P_2$ binding of ENTH-GFP in living cells, we then turned to voltage-sensitive PI 5-phosphatase from *Ciona intestinalis* (Ci-VSP) that is rapidly activated by membrane depolarization [48]. Upon voltage-dependent activation, Ci-VSP reversibly eliminates $PI(4,5)P_2$ and $PI(3,4,5)P_3$ from the membrane by dephosphorylation to PI(4)P and $PI(3,4)P_2$, respectively [18, 49]. We utilized Ci-VSP for titration of plasma membrane $PI(4,5)P_2$ levels to determine apparent affinities of the PI recognition domains [18, 23, 50]. This was done by gradual activation of Ci-VSP through depolarizing voltage steps under whole cell voltage clamp control, which sets $PI(4,5)P_2$ to distinct equilibrium concentrations at any given membrane potential [18, 23, 51]. Simultaneously, we measured membrane association of the PI binding domains in TIRF microscopy and obtained characteristic sigmoid fluorescence-voltage (F-V) curves (Figure 3E-G and Supplemental Figure 1B), as

previously reported for PLCδ1-PH-GFP and tubby$_{CT}$-GFP [18, 23]. From Boltzmann fits to these F-V curves, we calculated voltages of half-maximal sensor translocation (V_h) as quantitative measure for apparent PI(4,5)P_2 affinities of the PI binding domains [18]. Since stronger depolarization and correspondingly pronounced PI(4,5)P_2 depletion is required to induce sensor translocation, more positive V_h values represent higher PI(4,5)P_2 affinity in such experiments [18]. We compared apparent PI(4,5)P_2 affinities of ENTH-GFP (wild type, S4W mutant) with PLCδ1-PH-GFP and tubby$_{CT}$-GFP (wild type, R332H mutant). V_h values and apparent PI(4,5)P_2 affinities of ENTH-GFP were similar to tubby$_{CT}$-GFP (Figure 3E, H) and lower than that of PLCδ1-PH-GFP. Thus, PI(4,5)P_2 affinity of tubby$_{CT}$-GFP was lower than that of PLCδ1-PH-GFP [c.f. 18]. Introduction of a point mutation into ENTH-GFP and tubby$_{CT}$-GFP significantly shifted V_h to hyperpolarized membrane potentials demonstrating lower PI(4,5)P_2 affinity of the mutants (ENTH(S4W)-GFP: $P \leq 0.05$; Figure 3F, H; tubby$_{CT}$(R332H)-GFP: $P \leq 0.001$; Figure 3G, H). Accordingly, as suggested earlier, introduction of a single amino acid exchange indeed suffices to reduce the PI(4,5)P_2 binding affinity of these PI binding domains [11, 13].

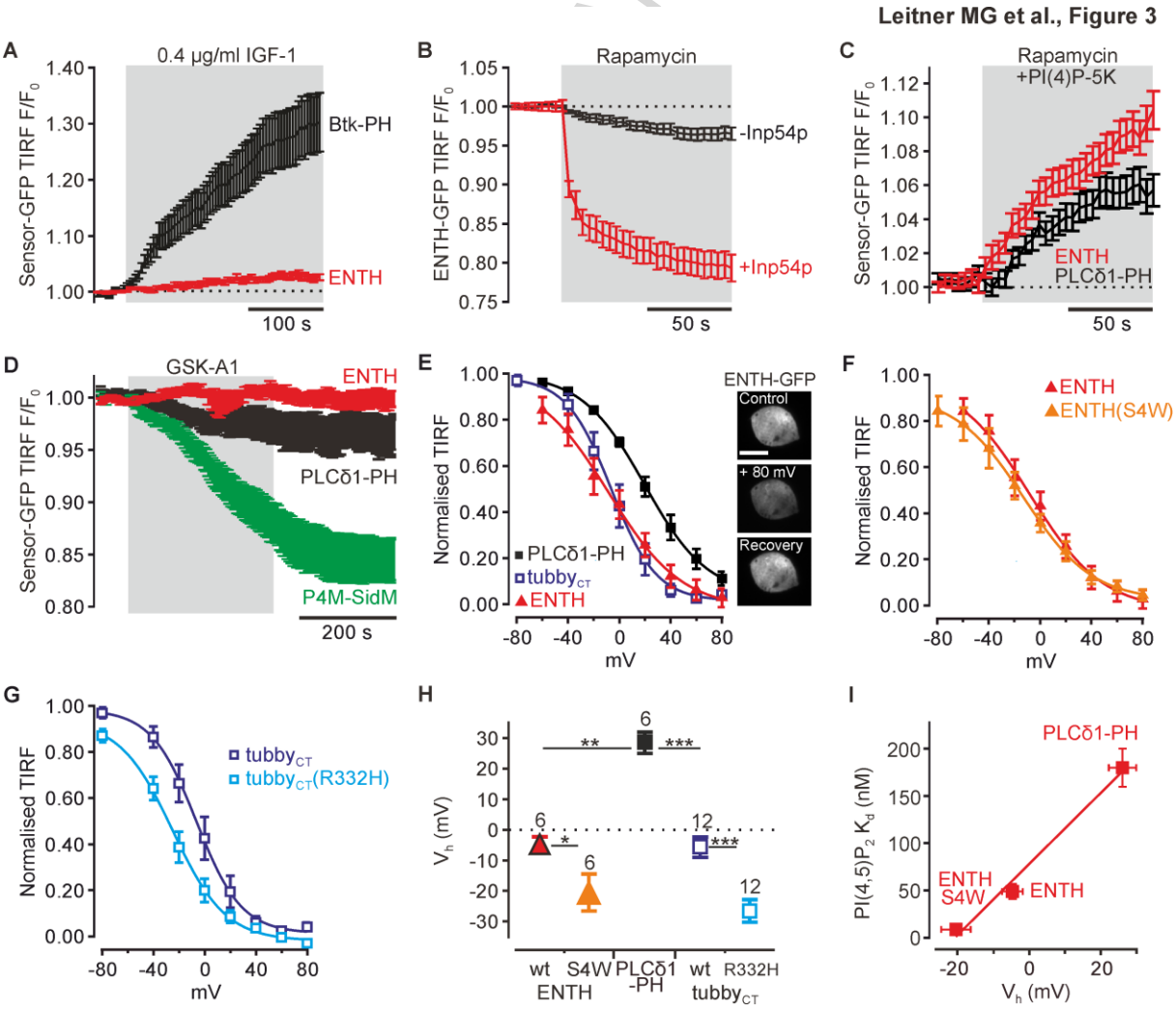

Figure 3. Specific binding of ENTH-GFP to PI(4,5)P_2 with low affinity in living cells.
(A) In CHO cells, Stimulation of endogenous receptors with IGF-1 (0.4 µg/ml, *grey inset*) increased membrane association of PI(3,4,5)P_3-specific probe Btk-PH-GFP (n=31). In contrast, membrane localization of ENTH-GFP (n=64) was not affected by application of IGF-1.
(B) Rapamycin-dependent recruitment of Inp54p to the plasma membrane induced membrane dissociation of ENTH-GFP (+Inp54p; n=35). Note slight rapamycin-induced translocation of ENTH-GFP independent on Inp54p (-Inp54p; n=71). **(C)** Membrane recruitment of PI(4)P-5K through application of rapamycin increased membrane association of ENTH-GFP (*red*; n=42) and PLCδ1-PH-GFP (*black*; n=27). This increase of membrane association was significantly pronounced for ENTH-GFP compared to PLCδ1-PH-GFP ($P \leq 0.05$; values after 100 s of rapamycin application were compared). Grey inserts in (B) and (C) indicate extracellular application of 5 µM rapamycin to cells transfected with ENTH-GFP, Lyn11-FRB and (B) Inp54p-FKBP or (C) PI(4)P-5K-FKBP. **(D)** Application of GSK-A1 (10 nM) induced rapid membrane dissociation of PI(4)P-specific probe P4M-SidM-GFP (n=14; $P \leq 0.001$ compared to base line; paired Student´s test). Membrane association of PLCδ1-PH-GFP (n=11) and ENTH-GFP (n=11) was not affected by treatment of cells with GSK-A1 (10 nM). **(E-H)** Titration of membrane PI(4,5)P_2 using Ci-VSP to quantify apparent PI(4,5)P_2 affinities of PI binding domains. Relative TIRF intensity was measured in response to stepwise depolarization of cells from -60 mV to +80 mV co-expressing RFP-labelled Ci-VSP and PI binding domains (see also Supplemental Figure 1B). **(E, F, G)** show steady-state F-V relations for cells co-expressing Ci-VSP together with GFP-labelled (E) PLCδ1-PH (n=6), $tubby_{CT}$ (n=12) or ENTH (n=6), (F) ENTH or ENTH(S4W) (n=6) and (G) $tubby_{CT}$ or $tubby_{CT}$(R332H) (n=12). Data for ENTH and $tubby_{CT}$ are reproduced in panels (E+F) and (E+G), respectively. Data were normalized as described in "Material and Methods". Continuous lines represent a Boltzmann fit calculated from averaged parameters derived from single recordings. For parameters of fits see Table 1. **(H)** shows summarized V_h values calculated from Boltzmann fits to F-V recordings shown in (E-G). **(I)** Apparent PI(4,5)P_2 binding affinities for PLCδ1-PH-GFP, ENTH-GFP and ENTH(S4W)-GFP deduced from Ci-VSP experiments correlated well with recently reported PI(4,5)P_2 K_d (nM) values (in vitro data from [19]).

Based on these findings, the rank order of apparent PI(4,5)P_2 binding affinities of the PI recognition domains was: PLCδ1-PH-GFP > ENTH-GFP ≈ $tubby_{CT}$-GFP > ENTH(S4W)-GFP ≈ $tubby_{CT}$(R332H)-GFP (Figure 3H). Thus, PLCδ1-PH-GFP displayed highest V_h values and highest apparent PI(4,5)P_2 affinity of all sensors tested. As shown in Figure 3I, apparent PI(4,5)P_2 affinities of ENTH-GFP, ENTH(S4W)-GFP and PLCδ1-PH-GFP obtained by utilizing Ci-VSP to titrate PI(4,5)P_2 levels in living cells correlated well with previously reported binding properties derived from *in vitro* assays [in vitro data from 19].

Table 1: Summarised parameters of Boltzmann fits presented in Figure 3E-G (mean ±SEM)

PI recognition domain	V_h (mV)	s (mV)	number of cells
PLCδ1-PH-GFP	26.05 ±3.84	27.46 ±2.53	6
ENTH-GFP	-6.42 ±3.76	29.13 ±7.10	6
ENTH(S4W)-GFP	-20.56 ±6.50	33.27 ±5.73	6
$tubby_{CT}$	-5.68 ±6.03	12.63 ±1.07	12

tubby$_{CT}$(R332H)	-26.54 ±4.14	15.81 ±3.18	12

3.5 ENTH-GFP reports on stimulation of PLCβ at low G_qPCR agonist concentrations

The observed low PI(4,5)P_2 affinity of ENTH-GFP in living cells should translate into high sensitivity of this biosensor to physiological PI(4,5)P_2 dynamics. To test this prediction, we again made use of m1R/PLCβ signaling as experimental model taking Oxo-M dose-response relations as measure for sensor sensitivity towards G_qPCR stimulation (Figure 4). We found that dissociation of ENTH-GFP was already apparent at low Oxo-M concentrations and half-maximal translocation occurred at an agonist concentration (EC_{50}) of about 0.1 µM (0.096 ±0.102 µM, n=35; Figure 4A-C). In agreement with the higher apparent PI(4,5)P_2 binding affinity, the EC_{50} for Oxo-M of PLCδ1-PH-GFP was significantly higher (EC_{50}=0.453 ±0.096 µM, n=44; P≤0.01; Figure 4A-C) than that of ENTH-GFP. Notably, PLCδ1-PH-GFP responded to G_qPCR stimulation at similarly low Oxo-M concentrations. However, the PLCδ1-PH-GFP response is likely to reflect an IP_3 increase rather than actual PI(4,5)P_2 dynamics.

We additionally compared ENTH-GFP and PLCδ1-PH-GFP with KCNQ ion channels as well-studied examples of PI(4,5)P_2-dependent proteins. Under the same experimental conditions, the Oxo-M sensitivity of homomeric KCNQ2 channels, known as particularly low-affinity PI(4,5)P_2-effectors [34, 36, 51], was very similar to the sensitivity of ENTH-GFP (EC_{50}=0.164 ±0.050 µM; n=5; Figure 4C; Supplemental Figure 1A). In comparison, m1R/Oxo-M sensitivity of heteromeric KCNQ2/3 channels characterized by higher PI(4,5)P_2 affinity was comparable to PLCδ1-PH-GFP responses (Figure 4C; Supplemental Figure 1A). In conclusion, the low effective PI(4,5)P_2 affinity makes ENTH-GFP a sensor particularly useful for moderate – yet probably physiologically relevant – PI(4,5)P_2 depletion through stimulation of G_qPCR.

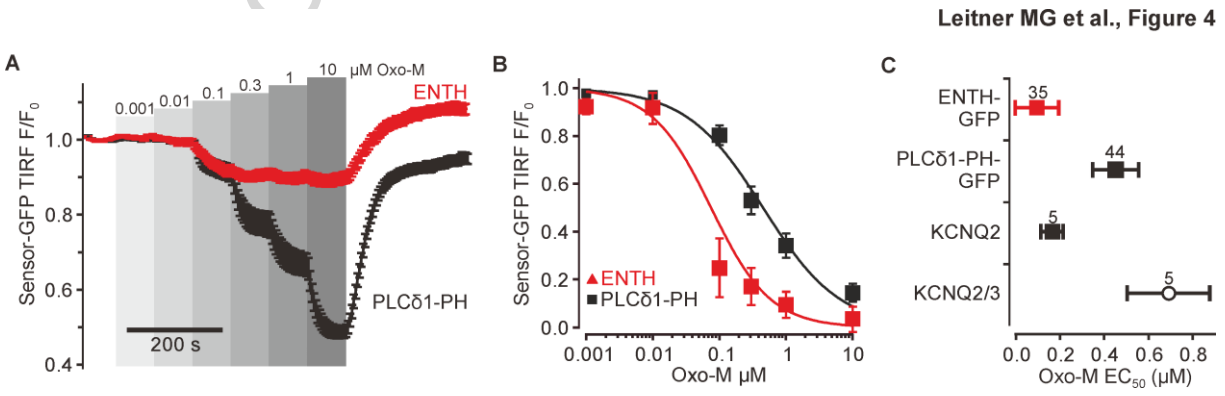

Figure 4. High sensitivity of ENTH-GFP to physiological PI(4,5)P_2 dynamics. (A) Membrane association of PI(4,5)P_2 sensors was measured in TIRF microscopy during stimulation of m1R with increasing Oxo-M concentrations. The panel shows mean time

course of membrane association of ENTH-GFP (n=35) and PLCδ1-PH-GFP (n=44) in these experiments. **(B+C)** Fluorescence intensity responses in experiments as shown in (A) were fitted to a Hill equation (solid lines) to calculate EC_{50} values for Oxo-M application as quantitative measure for sensor sensitivity to stimulation of m1R. **(C)** Summary of EC_{50} values (Oxo-M) for ENTH-GFP and PLCδ1-PH-GFP in comparison to m1R-induced inhibition of homomeric KCNQ2 (n=5) and heteromeric KCNQ2/3 (n=5) K^+ channels (c.f. Supplemental Figure 1A for KCNQ channel recordings). ENTH-GFP exhibited significantly lower Oxo-M EC_{50} values than PLCδ1-PH-GFP ($P \leq 0.01$) that were comparable to KCNQ2 channels.

3.6 Overexpression of ENTH-GFP does not affect cellular PI signaling

Overexpression of $tubby_{CT}$ and PLCδ1-PH-GFP has been shown to affect cellular PI signaling by reducing accessibility of $PI(4,5)P_2$ to PLCβ and thereby suppressing downstream signals [3, 12, 13]. We thus tested whether ENTH-GFP also exhibited such limitations. Therefore, we measured m1R-mediated suppression of KCNQ2 channels making use of the channel's particularly high sensitivity to $PI(4,5)P_2$ changes [36, 41, 51]. The reduction in current amplitude following sub-saturating activation of co-expressed m1R (stimulated with 100 nM Oxo-M) was our readout for efficacy of PLCβ/$PI(4,5)P_2$ signaling, while basal current amplitudes under resting conditions (and associated resting membrane potential) were used as sensitive measure for availability of free $PI(4,5)P_2$.

As shown in Figure 5A, 100 nM Oxo-M caused reversible inhibition of homomeric KCNQ2 channels by about 50% in control cells in absence of co-expressed sensor domains [30, 36]. Co-expression of PLCδ1-PH-GFP completely abolished inhibition of KCNQ2 channels through m1R stimulated with 100 nM Oxo-M (n=5; $P<0.001$; Figure 5A). Furthermore, basal current amplitudes were significantly reduced in cells co-expressing PLCδ1-PH-GFP compared to control cells without co-expressed biosensor (-Sensor; Figure 5B; $P<0.05$), and resting membrane potentials of cells expressing PLCδ1-PH-GFP were also significantly depolarized compared to (-Sensor) controls (Figure 5C; $P<0.01$). These findings indicated that overexpression of PLCδ1-PH-GFP reduced resting $PI(4,5)P_2$ levels available to KCNQ2 channels and attenuated PLCβ-dependent $PI(4,5)P_2$ dynamics. In contrast, when ENTH-GFP was co-expressed, KCNQ2 current suppression by receptor activation (n=7; Figure 5A), basal KCNQ2 currents (Figure 5B), and resting membrane potentials (Figure 5C) were unchanged with respect to (-Sensor) controls (no significant difference). In analogous experiments, co-expression with $tubby_{CT}$(R332H)-GFP also did not affect PLCβ-induced $PI(4,5)P_2$ dynamics or KCNQ2-mediated currents and membrane potentials (Figure 5A-C).

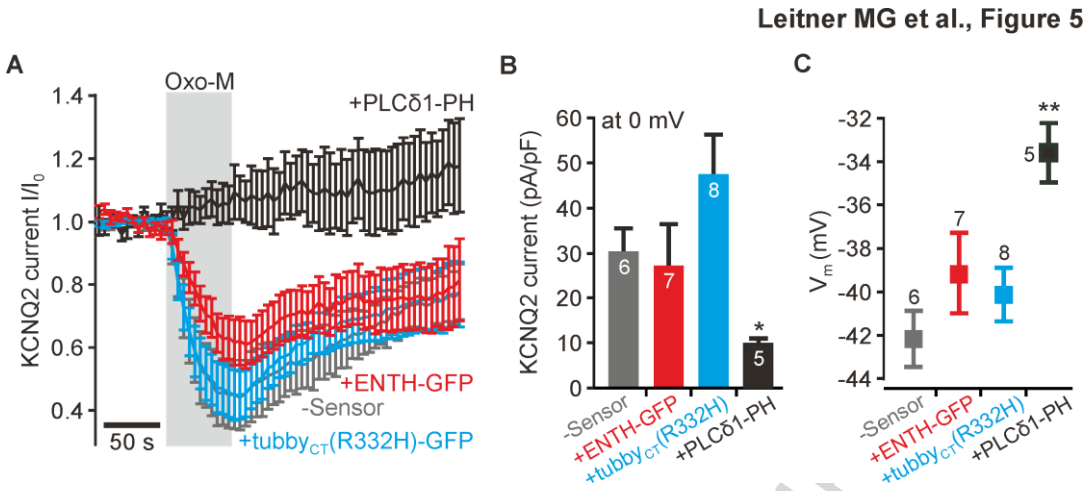

Figure 5. Overexpression of ENTH-GFP does not affect cellular PLCβ/PI(4,5)P_2 signaling.
(A) In cells co-expressing ENTH-GFP (n=7; *red*) or tubby$_{CT}$(R332H) (n=8; *blue*) m1R-mediated inhibition of homomeric KCNQ2 channels was comparable to control cells (n=6; *grey*). In contrast, expression of PLCδ1-PH-GFP completely abolished m1R-dependent inhibition of KCNQ2 channels (n=5; *black*) (grey inset indicates application of 100 nM Oxo-M). The panel shows the summarized time courses of m1R-induced KCNQ2 channel inhibition. **(B+C)** In contrast to PLCδ1-PH-GFP, co-expression of ENTH-GFP or tubby$_{CT}$(R322H) did not alter **(B)** KCNQ2 current amplitudes and **(C)** resting membrane potentials (statistical analysis was performed with Dunnett test in comparison with -*Sensor* controls; *P≤0.05, **P≤0.01).

Thus, in addition to its high sensitivity to PI(4,5)P_2 concentration changes, the relatively low affinity ENTH-PH endows this sensor with the advantage of minimal interference with endogenous PI(4,5)P_2 signaling.

4. DISCUSSION

The importance and diversity of cellular processes regulated by PI(4,5)P_2 has led to a strong need for sensors of PI(4,5)P_2 concentrations and concentration changes usable in live-cell experiments. PLCδ1-PH and tubby$_{CT}$ are established experimental biosensors and have been used successfully to address PI(4,5)P_2-dependent processes [e.g. 3, 4, 8, 11, 13, 52]. However, as PLCδ1-PH and tubby$_{CT}$ responses do not necessarily report on PLC-dependent PI(4,5)P_2 dynamics and as both domains apparently interfere with cellular PI metabolism [3, 11-13], there is clear demand for more sensitive and reliable PI(4,5)P_2 reporters. Yoon and colleagues introduced Epsin1-ENTH domain [20, 53-55] as live-cell reporter for PI(4,5)P_2 by labeling this domain with a fluorophore that is sensitive to changes in lipid surrounding [19]. Whilst this elegant approach allowed for quantitative analysis of PI(4,5)P_2 dynamics, its applicability might be limited, since introduction of the probe via microinjection appears incompatible with many experimental settings. Searching for a more general approach, we established ENTH

fused to GFP as genetically-encoded biosensor. We found that in living cells ENTH-GFP (i) specifically binds membrane PI(4,5)P_2, (ii) exhibits low apparent PI(4,5)P_2 affinity, (iii) does not affect cellular PI signaling and (iv) is highly sensitive to activation of G_qPCR and thus physiological depletion of PI(4,5)P_2.

4.1 ENTH-GFP specifically recognizes membrane PI(4,5)P_2

We characterized PI binding properties of ENTH-GFP in living cells utilizing genetically-encoded tools to experimentally manipulate PI concentrations. The responses of ENTH-GFP to the experimental interventions demonstrated specific binding of this biosensor to membrane PI(4,5)P_2: ENTH-GFP translocated into the cytoplasm during rapamycin-induced depletion of PI(4,5)P_2 through 5-phosphatase Inp54p and associated to the membrane during recruitment of PI(4)P-5K that produces PI(4,5)P_2 from PI(4)P [41, 42, 48]. Furthermore, the reporter dissociated from the membrane during activation of Ci-VSP. It is worth noting that, although the enzyme processes both PI(4,5)P_2 and PI(3,4,5)P_3 [18, 48], PI(4,5)P_2 was the main substrate of Ci-VSP in these experiments due to very low resting levels of PI(3,4,5)P_3 [18, 51]. These data unequivocally demonstrated that ENTH-GFP recognizes membrane PI(4,5)P_2. Moreover, these results showed absence of relevant binding of ENTH-GFP to PI(4)P and PI(3,4)P_2, as recruitment of Inp54p and activation of Ci-VSP strongly increase membrane PI(4)P and PI(4)P/PI(3,4)P_2 levels, respectively [18, 41, 42, 48, 56], without inducing translocation of ENTH to the membrane. Furthermore, insensitivity to application of GSK-A1, an inhibitor of PI4IIIK [44-47], confirmed that membrane association of ENTH-GFP does not involve binding to PI(4)P. Likewise, ENTH-GFP was insensitive to IGF-1-dependent stimulation of PI(3,4,5)P_3 and PI(3,4)P_2 signaling [39], indicating that interaction with both PI(3,4,5)P_3 and PI(3,4)P_2 is negligible in living cells. It seems worth pointing out that in vitro binding assays revealed some interaction of the ENTH domain with PI(3,4)P_2 and PI(3,4,5)P_3 [19]. The present results therefore emphasize that such biochemical in vitro assays do not necessarily reflect the binding behavior at more complex native plasma membranes in living cells, as also shown for other PI recognition domains previously [20, 37, 38]. Based on our findings, we thus conclude that in living cells ENTH-GFP specifically recognizes membrane PI(4,5)P_2.

4.2 ENTH-GFP has low PI(4,5)P_2 affinity

Using Ci-VSP to titrate membrane PI(4,5)P_2 levels [18, 23], we found that the PI(4,5)P_2 affinity of ENTH-GFP was similar to tubby$_{CT}$, but lower than that of PLCδ1-PH-GFP. These conclusions are supported by several other lines of evidence: (i) A recent study demonstrated that in vitro the PI(4,5)P_2 affinity of ENTH-GFP was lower than that of PLCδ1-PH [19].

(ii) Using confocal microscopy and TIRF imaging, we found that membrane association of ENTH-GFP under resting conditions, and hence translocation amplitudes of ENTH-GFP in response to $PI(4,5)P_2$ depletion were smaller than that of PLCδ1-PH-GFP. (iii) Membrane association of ENTH-GFP during PI(4)P-5K-mediated $PI(4,5)P_2$ synthesis increased significantly stronger than membrane localization of PLCδ1-PH-GFP. And (iv) in contrast to PLCδ1-PH-GFP, ENTH-GFP did not interfere with cellular $PI(4,5)P_2$ signaling indicating that the construct did not significantly compete with cellular proteins for $PI(4,5)P_2$ binding. Taken together, the behavior of ENTH-GFP in living cells can be fully explained by this low affinity for membrane $PI(4,5)P_2$.

4.3 A comparison of ENTH-GFP with established $PI(4,5)P_2$ biosensors

The most widely used biosensor for G_qPCR signaling, PLCδ1-PH, is a general sensor of PLC activity rather than a reporter of actual $PI(4,5)P_2$ depletion due to binding of IP_3 [3, 8, 9, 15, 28], although it appears to faithfully follow $PI(4,5)P_2$ concentration dynamics in the absence of IP_3 production [18, 43]. ENTH-GFP recapitulates $PI(4,5)P_2$ binding specificity of PLCδ1-PH-GFP, but as an important advantage [e.g. 11, 12-14], the construct is not sensitive to cytoplasmic IP_3. Thus, ENTH-GFP may be highly useful as a complementary $PI(4,5)P_2$ sensor to unequivocally correlate physiological processes to $PI(4,5)P_2$ level changes, specifically during activation of G_qPCR.

As far as $tubby_{CT}$ is concerned, the $PI(4,5)P_2$ binding properties and the behavior in living cells are not well understood. While $tubby_{CT}$ in vitro additionally binds $PI(3,4)P_2$ and $PI(3,4,5)P_3$ [10], in the cell, its membrane association seems to be largely independent of 3-phosphorylated PIs. This may be explained by the much higher cellular $PI(4,5)P_2$ levels compared to $PI(3,4)P_2$ and $PI(3,4,5)P_3$ [18, 57]. Conflicting evidence exists concerning tubby's $PI(4,5)P_2$ affinity: under resting conditions, $tubby_{CT}$ exhibits even stronger membrane association than PLCδ1-PH [13], and $tubby_{CT}$ frequently does not dissociate from the membrane upon activation of G_qPCR under conditions that should result in substantial $PI(4,5)P_2$ depletion (c.f. Figure 1 and [11-13]). These findings have been taken to estimate that the $PI(4,5)P_2$ affinity of $tubby_{CT}$ was higher than that of PLCδ1-PH and in fact too high to reliably detect physiological $PI(4,5)P_2$ changes [11, 13]. Accordingly and consistent with lowered $PI(4,5)P_2$ affinity, a single amino acid exchange (R332H) in the PI binding pocket renders $tubby_{CT}$ responsive to G_qPCR activity and reduces resting membrane association (Fig. 1 [11, 13]). However, present and previous data [see also 18, 57] obtained by titrating $PI(4,5)P_2$ through Ci-VSP show that the apparent $PI(4,5)P_2$ affinity of $tubby_{CT}$ is actually low, similar to ENTH-GFP and substantially lower than that of PLCδ1-PH. According to these

live-cell assays, the $PI(4,5)P_2$ affinity of $tubby_{CT}$ cannot be too high to detect G_qPCR-triggered $PI(4,5)P_2$ dynamics. In fact, activation of endogenous muscarinic receptors causes robust translocation of $tubby_{CT}$ in organotypic and dissociated cultures of hippocampal neurons [7, 12]. One tentative explanation for the contradictory observations concerning $tubby_{CT}$ is that while its $PI(4,5)P_2$ affinity is low, membrane association is co-determined by another interaction in a cell-type-specific manner, such that sensitivity to G_qPCR activation does not correspond to its actual $PI(4,5)P_2$ affinity. This line of thought is supported by the early finding that tubby protein physically interacts with $G\alpha_q$ proteins [10], and by the transient increase of $tubby_{CT}$ membrane association during G_qPCR stimulation observed in our experiments (Figure 1D). Taken together, the reliability of $tubby_{CT}$ as a sensor for $PI(4,5)P_2$ is questionable and further work is needed to elucidate the behavior of $tubby_{CT}$ during stimulation of G_qPCR. In contrast, ENTH-GFP responses in living cells are fully consistent with its $PI(4,5)P_2$ affinity and its membrane association reliably reports on PLCβ-mediated $PI(4,5)P_2$ depletion. We thus conclude that ENTH-GFP can be considered a reliable and specific biosensor for membrane-associated $PI(4,5)P_2$ that offers important advantages over PLCδ1-PH and $tubby_{CT}$.

4.4 Usage of ENTH-PH as biosensor for $PI(4,5)P_2$ in physiological pathways

As for voltage-dependent KCNQ2 channels [36], low affinity and high specificity for $PI(4,5)P_2$ facilitates high sensitivity of ENTH-GFP to stimulation of G_qPCR even at lowest agonist concentrations. Overexpression of ENTH-GFP does not interfere with cellular $PI(4,5)P_2$ signaling, in contrast to $PLC_{\delta1}$-PH-GFP that attenuated $PI(4,5)P_2$ levels at rest and PLCβ-dependent $PI(4,5)P_2$ dynamics [12, 13]. Just as for $tubby_{CT}$(R332H), $PI(4,5)P_2$ affinity of ENTH-GFP probably is too low to compete significantly for $PI(4,5)P_2$ binding with PLCβ or other cellular proteins (such as KCNQ2 channels in our experiments). On top of desired sensitivity of biosensors, this integrity is especially important when measurements of physiological $PI(4,5)_2$ dynamics are the experimental goal. Thus, ENTH-GFP appears suitable as biosensor highly sensitive to alterations of $PI(4,5)P_2$ during minimal activation of the receptor. ENTH-GFP indeed may be used to address small alterations of $PI(4,5)P_2$ through minute activation of PLCβ in physiological, possibly also native, settings. In this respect, our work not only established ENTH-GFP as reliable biosensor, but also showed that stimulation of m1R with Oxo-M at concentrations as low as 0.1 µM indeed caused substantial depletion of membrane $PI(4,5)P_2$ (see Figure 4). Furthermore, our findings highlight that combinatorial analysis of different $PI(4,5)P_2$ reporters under the same experimental condition constitutes a very useful strategy to experimentally assess G_qPCR-dependent $PI(4,5)P_2$ dynamics. As

responses of PI sensors may not exclusively depend on $PI(4,5)P_2$ levels (c.f. $tubby_{CT}$), analysis of structurally-unrelated biosensors (e.g. ENTH-GFP and PLCδ1-PH-GFP) that most probably are not affected by the same $PI(4,5)P_2$-independent mechanisms might reduce risk for misleading interpretations of results.

We want to point out that low membrane association under resting conditions and the low dynamic range of responses associated with its low $PI(4,5)P_2$ affinity constitute potential drawbacks of ENTH-GFP. Low degree of membrane association might limit use of ENTH-GFP under certain experimental conditions, as detectable translocation amplitudes depend on initial amounts of sensor at the plasma membrane. Indeed, ENTH-GFP responses during $PI(4,5)P_2$ depletion were small compared to PLCδ1-PH-GFP. However, membrane dissociation of ENTH-GFP during G_qPCR stimulation was readily detectable in TIRF microscopy, and a corresponding increase of sensor-associated fluorescence could be measured in the cytoplasm even with confocal microscopy despite high basal sensor abundance in the cytoplasm (c.f. Figure 1). Due to the small dynamic range of ENTH-GFP (c.f. Figure 4), it may be experimentally challenging to detect gradual ENTH-GFP responses and accordingly it may be difficult to monitor gradual changes of $PI(4,5)P_2$ depletion during activation of PLCβ using ENTH-GFP as read-out. However, G_qPCR-dependent translocation of ENTH-GFP was comparable to $tubby_{CT}$(R332H) that has been utilized successfully in several cell types [58-60]. Importantly, low membrane association of ENTH-GFP also offers a relevant advantage, as the sensor is particularly suitable for detection of (local) increases in membrane $PI(4,5)P_2$. Indeed, ENTH-GFP was more sensitive to $PI(4,5)P_2$ synthesis than PLCδ1-PH-GFP (c.f. Figure 3C) proposing ENTH-GFP also as reliable reporter for $PI(4,5)P_2$ level increases in the membrane, such as those associated with synaptic vesicle release or cell migration [1].

4.5 Conclusion

We conclude that ENTH-GFP qualifies as reliable genetically-encoded biosensor of physiological $PI(4,5)P_2$ dynamics that offers certain advantages over established biosensors. As ENTH-GFP responses can be utilized to correlate physiological $PI(4,5)P_2$ dynamics to cellular processes, the reporter constitutes important complementation of the available repertoire of reporters to monitor $PI(4,5)P_2$ signaling.

Acknowledgements and grant support

The authors acknowledge the kind gifts of plasmids for Ci-VSP from Y. Okamura, $tubby_{CT}$ from L. Shapiro, PLCδ1-PH-GFP and the rapamycin recruitment system from T. Meyer, Epsin1-ENTH from W. Cho, Btk-PH-GFP and P4M-SidM-GFP from T. Balla and KCNQ2/3

from T.J. Jentsch. We thank Natalia Fritzler and Olga Ebers for excellent technical assistance. We want to thank the reviewers for very insightful, detailed, and constructive comments on our manuscript. This work was supported by Research Grants of the University Medical Center Giessen und Marburg (UKGM) to M.G.L. (UKGM17/2013 and UKGM13/2016) and by the German Research Foundation (DFG) through Priority Program 1608: ”Ultrafast and temporally precise information processing: Normal and dysfunctional hearing” (LE 3600/1-1 to MGL) and through Sonderforschungsbereich (SFB) 593 (TPA12 to DO).

Author contributions

M.G.L and D.O conceived the project, designed experiments, analyzed data and wrote the paper; M.G.L, B.U.W, V.T, V.N, Y.K, and C.R.H collected, analyzed and interpreted data. All authors approved the final version of the manuscript and all authors that qualify for authorship are designated.

Competing interest

The authors declare that they have no competing interest

REFERENCES

[1] T. Balla, Phosphoinositides: tiny lipids with giant impact on cell regulation, Physiological reviews, 93 (2013) 1019-1137.

[2] G. Di Paolo, P. De Camilli, Phosphoinositides in cell regulation and membrane dynamics, Nature, 443 (2006) 651-657.

[3] D. Raucher, T. Stauffer, W. Chen, K. Shen, S. Guo, J.D. York, M.P. Sheetz, T. Meyer, Phosphatidylinositol 4,5-bisphosphate functions as a second messenger that regulates cytoskeleton-plasma membrane adhesion, Cell, 100 (2000) 221-228.

[4] F. Giordano, Y. Saheki, O. Idevall-Hagren, S.F. Colombo, M. Pirruccello, I. Milosevic, E.O. Gracheva, S.N. Bagriantsev, N. Borgese, P. De Camilli, PI(4,5)P(2)-dependent and Ca(2+)-regulated ER-PM interactions mediated by the extended synaptotagmins, Cell, 153 (2013) 1494-1509.

[5] G. Kadamur, E.M. Ross, Mammalian phospholipase C, Annual review of physiology, 75 (2013) 127-154.

[6] T. Balla, P. Varnai, Visualization of cellular phosphoinositide pools with GFP-fused protein-domains, Curr Protoc Cell Biol, Chapter 24 (2009) Unit 24 24.

[7] M.G. Leitner, C.R. Halaszovich, O. Ivanova, D. Oliver, Phosphoinositide dynamics in the postsynaptic membrane compartment: Mechanisms and experimental approach, European journal of cell biology, 94 (2015) 401-414.

[8] T.P. Stauffer, S. Ahn, T. Meyer, Receptor-induced transient reduction in plasma membrane PtdIns(4,5)P2 concentration monitored in living cells, Current biology : CB, 8 (1998) 343-346.

[9] P. Varnai, T. Balla, Visualization of phosphoinositides that bind pleckstrin homology domains: calcium- and agonist-induced dynamic changes and relationship to myo-[3H]inositol-labeled phosphoinositide pools, The Journal of cell biology, 143 (1998) 501-510.

[10] S. Santagata, T.J. Boggon, C.L. Baird, C.A. Gomez, J. Zhao, W.S. Shan, D.G. Myszka, L. Shapiro, G-protein signaling through tubby proteins, Science, 292 (2001) 2041-2050.

[11] K.V. Quinn, P. Behe, A. Tinker, Monitoring changes in membrane phosphatidylinositol 4,5-bisphosphate in living cells using a domain from the transcription factor tubby, The Journal of physiology, 586 (2008) 2855-2871.

[12] C.P. Nelson, S.R. Nahorski, R.A. Challiss, Temporal profiling of changes in phosphatidylinositol 4,5-bisphosphate, inositol 1,4,5-trisphosphate and diacylglycerol allows comprehensive analysis of phospholipase C-initiated signalling in single neurons, Journal of neurochemistry, 107 (2008) 602-615.

[13] Z. Szentpetery, A. Balla, Y.J. Kim, M.A. Lemmon, T. Balla, Live cell imaging with protein domains capable of recognizing phosphatidylinositol 4,5-bisphosphate; a comparative study, BMC cell biology, 10 (2009) 67.

[14] M.S. Nash, K.W. Young, G.B. Willars, R.A. Challiss, S.R. Nahorski, Single-cell imaging of graded Ins(1,4,5)P3 production following G-protein-coupled-receptor activation, The Biochemical journal, 356 (2001) 137-142.

[15] K. Hirose, S. Kadowaki, M. Tanabe, H. Takeshima, M. Iino, Spatiotemporal dynamics of inositol 1,4,5-trisphosphate that underlies complex Ca2+ mobilization patterns, Science, 284 (1999) 1527-1530.

[16] J. van der Wal, R. Habets, P. Varnai, T. Balla, K. Jalink, Monitoring agonist-induced phospholipase C activation in live cells by fluorescence resonance energy transfer, The Journal of biological chemistry, 276 (2001) 15337-15344.

[17] I.N. Fleming, I.H. Batty, A.R. Prescott, A. Gray, G.S. Kular, H. Stewart, C.P. Downes, Inositol phospholipids regulate the guanine-nucleotide-exchange factor Tiam1 by facilitating its binding to the plasma membrane and regulating GDP/GTP exchange on Rac1, The Biochemical journal, 382 (2004) 857-865.

[18] C.R. Halaszovich, D.N. Schreiber, D. Oliver, Ci-VSP is a depolarization-activated phosphatidylinositol-4,5-bisphosphate and phosphatidylinositol-3,4,5-trisphosphate 5'-phosphatase, The Journal of biological chemistry, 284 (2009) 2106-2113.

[19] Y. Yoon, P.J. Lee, S. Kurilova, W. Cho, In situ quantitative imaging of cellular lipids using molecular sensors, Nature chemistry, 3 (2011) 868-874.

[20] T. Itoh, S. Koshiba, T. Kigawa, A. Kikuchi, S. Yokoyama, T. Takenawa, Role of the ENTH domain in phosphatidylinositol-4,5-bisphosphate binding and endocytosis, Science, 291 (2001) 1047-1051.

[21] G.R. Hammond, M.P. Machner, T. Balla, A novel probe for phosphatidylinositol 4-phosphate reveals multiple pools beyond the Golgi, The Journal of cell biology, 205 (2014) 113-126.

[22] M.G. Leitner, C.R. Halaszovich, D. Oliver, Aminoglycosides inhibit KCNQ4 channels in cochlear outer hair cells via depletion of phosphatidylinositol(4,5)bisphosphate, Molecular pharmacology, 79 (2011) 51-60.

[23] C.R. Halaszovich, M.G. Leitner, A. Mavrantoni, A. Le, L. Frezza, A. Feuer, D.N. Schreiber, C.A. Villalba-Galea, D. Oliver, A human phospholipid phosphatase activated by a transmembrane control module, Journal of lipid research, 53 (2012) 2266-2274.

[24] A.D. Edelstein, M.A. Tsuchida, N. Amodaj, H. Pinkard, R.D. Vale, N. Stuurman, Advanced methods of microscope control using muManager software, J Biol Methods, 1 (2014).

[25] M.G. Leitner, N. Michel, M. Behrendt, M. Dierich, S. Dembla, B.U. Wilke, M. Konrad, M. Lindner, J. Oberwinkler, D. Oliver, Direct modulation of TRPM4 and TRPM3 channels by the phospholipase C inhibitor U73122, British journal of pharmacology, 173 (2016) 2555-2569.

[26] M.G. Leitner, A. Feuer, O. Ebers, D.N. Schreiber, C.R. Halaszovich, D. Oliver, Restoration of ion channel function in deafness-causing KCNQ4 mutants by synthetic channel openers, British journal of pharmacology, 165 (2012) 2244-2259.

[27] M.N. Teruel, T.A. Blanpied, K. Shen, G.J. Augustine, T. Meyer, A versatile microporation technique for the transfection of cultured CNS neurons, Journal of neuroscience methods, 93 (1999) 37-48.

[28] L.F. Horowitz, W. Hirdes, B.C. Suh, D.W. Hilgemann, K. Mackie, B. Hille, Phospholipase C in living cells: activation, inhibition, Ca2+ requirement, and regulation of M current, J Gen Physiol, 126 (2005) 243-262.

[29] M.S. Shapiro, J.P. Roche, E.J. Kaftan, H. Cruzblanca, K. Mackie, B. Hille, Reconstitution of muscarinic modulation of the KCNQ2/KCNQ3 K(+) channels that underlie the neuronal M current, The Journal of neuroscience : the official journal of the Society for Neuroscience, 20 (2000) 1710-1721.

[30] B.C. Suh, B. Hille, Recovery from muscarinic modulation of M current channels requires phosphatidylinositol 4,5-bisphosphate synthesis, Neuron, 35 (2002) 507-520.

[31] M. Kruse, G.R. Hammond, B. Hille, Regulation of voltage-gated potassium channels by PI(4,5)P2, The Journal of general physiology, 140 (2012) 189-205.

[32] M. Kruse, B. Hille, The phosphoinositide sensitivity of the K(v) channel family, Channels (Austin), 7 (2013) 530-536.

[33] B.U. Wilke, M. Lindner, L. Greifenberg, A. Albus, Y. Kronimus, M. Bunemann, M.G. Leitner, D. Oliver, Diacylglycerol mediates regulation of TASK potassium channels by Gq-coupled receptors, Nature communications, 5 (2014) 5540.

[34] Y. Li, N. Gamper, D.W. Hilgemann, M.S. Shapiro, Regulation of Kv7 (KCNQ) K+ channel open probability by phosphatidylinositol 4,5-bisphosphate, The Journal of neuroscience : the official journal of the Society for Neuroscience, 25 (2005) 9825-9835.

[35] H. Zhang, L.C. Craciun, T. Mirshahi, T. Rohacs, C.M. Lopes, T. Jin, D.E. Logothetis, PIP(2) activates KCNQ channels, and its hydrolysis underlies receptor-mediated inhibition of M currents, Neuron, 37 (2003) 963-975.

[36] C.C. Hernandez, B. Falkenburger, M.S. Shapiro, Affinity for phosphatidylinositol 4,5-bisphosphate determines muscarinic agonist sensitivity of Kv7 K+ channels, J Gen Physiol, 134 (2009) 437-448.

[37] J.W. Yu, J.M. Mendrola, A. Audhya, S. Singh, D. Keleti, D.B. DeWald, D. Murray, S.D. Emr, M.A. Lemmon, Genome-wide analysis of membrane targeting by S. cerevisiae pleckstrin homology domains, Molecular cell, 13 (2004) 677-688.

[38] A. Balla, Y.J. Kim, P. Varnai, Z. Szentpetery, Z. Knight, K.M. Shokat, T. Balla, Maintenance of hormone-sensitive phosphoinositide pools in the plasma membrane requires phosphatidylinositol 4-kinase IIIalpha, Molecular biology of the cell, 19 (2008) 711-721.

[39] Q. Tong, N. Gamper, J.L. Medina, M.S. Shapiro, J.D. Stockand, Direct activation of the epithelial Na(+) channel by phosphatidylinositol 3,4,5-trisphosphate and phosphatidylinositol 3,4-bisphosphate produced by phosphoinositide 3-OH kinase, The Journal of biological chemistry, 279 (2004) 22654-22663.

[40] K. Salim, M.J. Bottomley, E. Querfurth, M.J. Zvelebil, I. Gout, R. Scaife, R.L. Margolis, R. Gigg, C.I. Smith, P.C. Driscoll, M.D. Waterfield, G. Panayotou, Distinct specificity in the recognition of phosphoinositides by the pleckstrin homology domains of dynamin and Bruton's tyrosine kinase, The EMBO journal, 15 (1996) 6241-6250.

[41] B.C. Suh, T. Inoue, T. Meyer, B. Hille, Rapid chemically induced changes of PtdIns(4,5)P2 gate KCNQ ion channels, Science, 314 (2006) 1454-1457.

[42] P. Varnai, B. Thyagarajan, T. Rohacs, T. Balla, Rapidly inducible changes in phosphatidylinositol 4,5-bisphosphate levels influence multiple regulatory functions of the lipid in intact living cells, The Journal of cell biology, 175 (2006) 377-382.

[43] M. Lindner, M.G. Leitner, C.R. Halaszovich, G.R. Hammond, D. Oliver, Probing the regulation of TASK potassium channels by PI4,5P(2) with switchable phosphoinositide phosphatases, The Journal of physiology, 589 (2011) 3149-3162.

[44] N. Bojjireddy, J. Botyanszki, G. Hammond, D. Creech, R. Peterson, D.C. Kemp, M. Snead, R. Brown, A. Morrison, S. Wilson, S. Harrison, C. Moore, T. Balla, Pharmacological and genetic targeting of the PI4KA enzyme reveals its important role in maintaining plasma membrane phosphatidylinositol 4-phosphate and phosphatidylinositol 4,5-bisphosphate levels, The Journal of biological chemistry, 289 (2014) 6120-6132.

[45] M. Sohn, P. Ivanova, H.A. Brown, D.J. Toth, P. Varnai, Y.J. Kim, T. Balla, Lenz-Majewski mutations in PTDSS1 affect phosphatidylinositol 4-phosphate metabolism at ER-PM and ER-Golgi junctions, Proceedings of the National Academy of Sciences of the United States of America, 113 (2016) 4314-4319.

[46] M. Sohn, M. Korzeniowski, J.P. Zewe, R.C. Wills, G.R.V. Hammond, J. Humpolickova, L. Vrzal, D. Chalupska, V. Veverka, G.D. Fairn, E. Boura, T. Balla, PI(4,5)P2 controls plasma membrane PI4P and PS levels via ORP5/8 recruitment to ER-PM contact sites, The Journal of cell biology, 217 (2018) 1797-1813.

[47] G. Gulyas, J.T. Toth, D.J. Toth, I. Kurucz, L. Hunyady, T. Balla, P. Varnai, Measurement of inositol 1,4,5-trisphosphate in living cells using an improved set of resonance energy transfer-based biosensors, PLoS One, 10 (2015) e0125601.

[48] Y. Murata, H. Iwasaki, M. Sasaki, K. Inaba, Y. Okamura, Phosphoinositide phosphatase activity coupled to an intrinsic voltage sensor, Nature, 435 (2005) 1239-1243.

[49] H. Iwasaki, Y. Murata, Y. Kim, M.I. Hossain, C.A. Worby, J.E. Dixon, T. McCormack, T. Sasaki, Y. Okamura, A voltage-sensing phosphatase, Ci-VSP, which shares sequence identity with PTEN, dephosphorylates phosphatidylinositol 4,5-bisphosphate, Proceedings of the National Academy of Sciences of the United States of America, 105 (2008) 7970-7975.

[50] J. Lacroix, C.R. Halaszovich, D.N. Schreiber, M.G. Leitner, F. Bezanilla, D. Oliver, C.A. Villalba-Galea, Controlling the activity of a phosphatase and tensin homolog (PTEN) by membrane potential, The Journal of biological chemistry, 286 (2011) 17945-17953.

[51] A. Rjasanow, M.G. Leitner, V. Thallmair, C.R. Halaszovich, D. Oliver, Ion channel regulation by phosphoinositides analyzed with VSPs-PI(4,5)P2 affinity, phosphoinositide selectivity, and PI(4,5)P2 pool accessibility, Frontiers in pharmacology, 6 (2015) 127.

[52] X. Zhang, S. Mak, L. Li, A. Parra, B. Denlinger, C. Belmonte, P.A. McNaughton, Direct inhibition of the cold-activated TRPM8 ion channel by Galphaq, Nature cell biology, 14 (2012) 851-858.

[53] H. Kim, H.S. Afsari, W. Cho, High-Throughput Fluorescence Assay for Quantifying Membrane-Protein Interaction and Screening Inhibitors for Membrane-Protein Interaction, Journal of lipid research, (2013).

[54] C.P. Ford, P.L. Stemkowski, P.A. Smith, Possible role of phosphatidylinositol 4,5 bisphosphate in luteinizing hormone releasing hormone-mediated M-current inhibition in bullfrog sympathetic neurons, Eur J Neurosci, 20 (2004) 2990-2998.

[55] J. Hyman, H. Chen, P.P. Di Fiore, P. De Camilli, A.T. Brunger, Epsin 1 undergoes nucleocytosolic shuttling and its eps15 interactor NH(2)-terminal homology (ENTH) domain, structurally similar to Armadillo and HEAT repeats, interacts with the transcription factor promyelocytic leukemia Zn(2)+ finger protein (PLZF), The Journal of cell biology, 149 (2000) 537-546.

[56] S. Yamaguchi, T. Kurokawa, I. Taira, N. Aoki, S. Sakata, Y. Okamura, K.J. Homma, Potential role of voltage-sensing phosphatases in regulation of cell structure through the production of PI(3,4)P2, J Cell Physiol, 229 (2014) 422-433.

[57] A. Mavrantoni, V. Thallmair, M.G. Leitner, D.N. Schreiber, D. Oliver, C.R. Halaszovich, A method to control phosphoinositides and to analyze PTEN function in living cells using voltage sensitive phosphatases, Frontiers in pharmacology, 6 (2015) 68.

[58] S. Hughes, S.J. Marsh, A. Tinker, D.A. Brown, PIP(2)-dependent inhibition of M-type (Kv7.2/7.3) potassium channels: direct on-line assessment of PIP(2) depletion by Gq-coupled receptors in single living neurons, Pflugers Archiv : European journal of physiology, 455 (2007) 115-124.

[59] R.C. Hardie, C.H. Liu, A.S. Randall, S. Sengupta, In vivo tracking of phosphoinositides in Drosophila photoreceptors, Journal of cell science, 128 (2015) 4328-4340.

[60] C.H. Liu, H.K. Chang, S.P. Lee, R.C. Shieh, Activation of the Ca(2+)-sensing receptors increases currents through inward rectifier K(+) channels via activation of phosphatidylinositol 4-kinase, Pflugers Archiv : European journal of physiology, 468 (2016) 1931-1943.

FIGURE LEGENDS

Figure 1. ENTH-GFP is a reliable biosensor of PLCβ activity in living cells.

(A) Confocal images of CHO cells transiently expressing Lyn11-RFP (*red*) together with PI recognition domains fused to GFP (*green*). We detected large amounts of ENTH-GFP, ENTH(S4W) and tubby$_{CT}$(R332H)-GFP in the cytoplasm of resting cells (all scale bars 10 µm). **(B)** In some cells, ENTH-GFP labelled rod-like intracellular structures (*see arrowheads*; images are the same as shown in (A); scale bar 10 µm). **(C)** Stimulation of m1R with Oxo-M (10 µM) induced robust and reversible membrane dissociation of ENTH-GFP (n=65) and ENTH(S4W)-GFP (n=45). **(D)** Membrane-association of PLCδ1-PH-GFP (n=25) and tubby$_{CT}$(R332H)-GFP (n=39) reversibly decreased in response to m1R activation. Tubby$_{CT}$-GFP (n=46) displayed a transient increase of membrane association during activation of m1R. Traces in (C+D) show mean time course of membrane binding recorded with TIRF microscopy. **(E)** Measured with TIRF microscopy, relative changes of membrane association of ENTH-GFP were bigger than for ENTH(S4W) ($P \leq 0.001$) and for tubby$_{CT}$ ($P \leq 0.001$),

similar to tubby$_{CT}$(R332H)-GFP (n.s, not significant) and smaller than for PLCδ1-PH-GFP (P≤0.001; changes of membrane association derived from experiments shown in (C) and (D)). **(F)** We detected a cytoplasmic increase of ENTH-GFP (n=14) and ENTH(S4W)-GFP (n=26) during activation of m1R using confocal microscopy to measure sensor location in the cytoplasm. Grey insets in (C), (D) and (F) indicate application of Oxo-M (10 µM).

Figure 2. Membrane association of ENTH-GFP is not affected by cytoplasmic IP_3.

(A) Membrane association of PI recognition domains was recorded with TIRF microscopy in cells dialyzed with intracellular solution containing 5 µM IP_3 through a patch pipette (see "Material and Methods" for details). **(B-D)** Even in absence of IP_3, membrane association of all sensors decreased upon establishment of the whole cell configuration (*black*, cells dialyzed with standard intracellular solution). The *arrowhead* in (B) and (C) indicates establishment of the whole cell configuration. **(B)** Membrane association of PLCδ1-PH-GFP decreased even further, when cells were dialyzed with pipette solution containing IP_3 (*red*). **(C)** membrane localization of ENTH-GFP was insensitive to cytoplasmic IP_3. **(D)** shows a summary of recordings as shown in (B) and (C). Membrane association of ENTH-GFP and tubby$_{CT}$ constructs was not affected by dialysis of cells with IP_3. Upon dialysis of cells with IP_3, membrane association of PLCδ1-PH-GFP significantly decreased (P≤0.001) and of ENTH(S4W)-GFP surprisingly increased (P≤0.05) (TIRF signals were analyzed after 5 min of dialysis of cells with control solution or with solution containing 5 µM IP_3 (*red*); numbers in (D) represent numbers of cells recorded for each experimental condition).

Figure 3. Specific binding of ENTH-GFP to $PI(4,5)P_2$ with low affinity in living cells.

(A) In CHO cells, Stimulation of endogenous receptors with IGF-1 (0.4 µg/ml, *grey inset*) increased membrane association of $PI(3,4,5)P_3$-specific probe Btk-PH-GFP (n=31). In contrast, membrane localization of ENTH-GFP (n=64) was not affected by application of IGF-1.

(B) Rapamycin-dependent recruitment of Inp54p to the plasma membrane induced membrane dissociation of ENTH-GFP (+Inp54p; n=35). Note slight rapamycin-induced translocation of ENTH-GFP independent on Inp54p (-Inp54p; n=71). **(C)** Membrane recruitment of PI(4)P-5K through application of rapamycin increased membrane association of ENTH-GFP (*red*; n=42) and PLCδ1-PH-GFP (*black*; n=27). This increase of membrane association was significantly pronounced for ENTH-GFP compared to PLCδ1-PH-GFP (P≤0.05; values after 100 s of rapamycin application were compared). Grey inserts in (B) and (C) indicate extracellular application of 5 µM rapamycin to cells transfected with ENTH-GFP, Lyn11-FRB and (B) Inp54p-FKBP or (C) PI(4)P-5K-FKBP. **(D)** Application of GSK-A1 (10 nM)

induced rapid membrane dissociation of PI(4)P-specific probe P4M-SidM-GFP (n=14; P≤0.001 compared to base line; paired Student´s test). Membrane association of PLCδ1-PH-GFP (n=11) and ENTH-GFP (n=11) was not affected by treatment of cells with GSK-A1 (10 nM). **(E-H)** Titration of membrane $PI(4,5)P_2$ using Ci-VSP to quantify apparent $PI(4,5)P_2$ affinities of PI binding domains. Relative TIRF intensity was measured in response to stepwise depolarization of cells from -60 mV to +80 mV co-expressing RFP-labelled Ci-VSP and PI binding domains (see also Supplemental Figure 1B). **(E, F, G)** show steady-state F-V relations for cells co-expressing Ci-VSP together with GFP-labelled (E) PLCδ1-PH (n=6), $tubby_{CT}$ (n=12) or ENTH (n=6), (F) ENTH or ENTH(S4W) (n=6) and (G) $tubby_{CT}$ or $tubby_{CT}$(R332H) (n=12). Data for ENTH and $tubby_{CT}$ are reproduced in panels (E+F) and (E+G), respectively. Data were normalized as described in "Material and Methods". Continuous lines represent a Boltzmann fit calculated from averaged parameters derived from single recordings. For parameters of fits see Table 1. **(H)** shows summarized V_h values calculated from Boltzmann fits to F-V recordings shown in (E-G). **(I)** Apparent $PI(4,5)P_2$ binding affinities for PLCδ1-PH-GFP, ENTH-GFP and ENTH(S4W)-GFP deduced from Ci-VSP experiments correlated well with recently reported $PI(4,5)P_2$ K_d (nM) values (in vitro data from [19]).

Figure 4. High sensitivity of ENTH-GFP to physiological $PI(4,5)P_2$ dynamics. **(A)** Membrane association of $PI(4,5)P_2$ sensors was measured in TIRF microscopy during stimulation of m1R with increasing Oxo-M concentrations. The panel shows mean time course of membrane association of ENTH-GFP (n=35) and PLCδ1-PH-GFP (n=44) in these experiments. **(B+C)** Fluorescence intensity responses in experiments as shown in (A) were fitted to a Hill equation (solid lines) to calculate EC_{50} values for Oxo-M application as quantitative measure for sensor sensitivity to stimulation of m1R. **(C)** Summary of EC_{50} values (Oxo-M) for ENTH-GFP and PLCδ1-PH-GFP in comparison to m1R-induced inhibition of homomeric KCNQ2 (n=5) and heteromeric KCNQ2/3 (n=5) K^+ channels (c.f. Supplemental Figure 1A for KCNQ channel recordings). ENTH-GFP exhibited lower Oxo-M EC_{50} values than PLCδ1-PH-GFP that were comparable to KCNQ2 channels.

Figure 5. Overexpression of ENTH-GFP does not affect cellular PLCβ/$PI(4,5)P_2$ signaling.

(A) In cells co-expressing ENTH-GFP (n=7; *red*) or $tubby_{CT}$(R332H) (n=8; *blue*) m1R-mediated inhibition of homomeric KCNQ2 channels was comparable to control cells (n=6; *grey*). In contrast, expression of PLCδ1-PH-GFP completely abolished m1R-dependent inhibition of KCNQ2 channels (n=5; *black*) (grey inset indicates application of 100 nM Oxo-

M). The panel shows the summarized time courses of m1R-induced KCNQ2 channel inhibition. **(B+C)** In contrast to PLCδ1-PH-GFP, co-expression of ENTH-GFP or tubby$_{CT}$(R322H) did not alter **(B)** KCNQ2 current amplitudes and **(C)** resting membrane potentials (statistical analysis was performed with Dunnett test in comparison with -*Sensor* controls; *P≤0.05, **P≤0.01).

Highlights Leitner et al. (BBALIP-18-77)

• Fluorescently-labelled N-terminal homology domain of epsin1 (ENTH-GFP) binds membrane PI(4,5)P_2 with low affinity and high specificity

• ENTH-GFP membrane association can be monitored easily with standard microscopic techniques

• ENTH-GFP translocates from the membrane into cytoplasm during activation of G_q protein-coupled receptors

• Overexpression of ENTH-GFP does not affect PI(4,5)P_2 metabolism and signalling

• ENTH-GFP is a reliable genetically-encoded reporter of physiological PI(4,5)P_2 dynamics